JOURNAL OF THERMOPHYSICS AND HEAT TRANSFER
Vol. 20, No. 3, July–September 2006

# Thermal Joint Conductance of Low-Density Polyethylene and Polyester Polymeric Films: Experimental

Ick-Chan Kim,* E. E. Marotta,† and L. S. Fletcher‡
*Texas A&M University, College Station, Texas 77840-3123*

**The flow of thermal energy across a joint where one or more surfaces come into contact is an important engineering consideration. Studies of metal/metal contacts at an interface have been investigated extensively and are well documented in the literature. Although equally important in many engineering application, the study of nonmetallic or organic contacting surfaces is still in its infancy. Currently, an elastic model exists for predicting the thermal performance of metal/polymer joints. In addition, a plastic model was recently proposed to account for plastic deformation of the contacting asperities. Both thermal contact models have been compared to experimental polymer layers that are relatively thick. The present objective was to investigate experimentally two commercially important polymeric film types for thermal conductance ranging from 254 to 12.2 $\mu$m in thickness under interface pressures varied from 103.4 (15) to 23,774.5 kPa (3450 psi). In each of the experimental tests, the ambient fluid at the contacting interface was air. One other objective was to conduct film nanoindentation measurements to possibly deduce a microdeformation mode. Surface metrology and film morphology are presented with a goal to incorporate these results into future modeling endeavors. The polymeric films investigated were low-density polyethylene and polyester, for example, Mylar®.**

## Nomenclature

| | | |
|---|---|---|
| $A_a$ | = | apparent contact area, m$^2$ |
| $A_t$ | = | true contact area at maximum load/penetration, m$^2$ |
| $d$ | = | distance between atoms, m |
| $E$ | = | Young's modulus, GPa |
| $F$ | = | applied force, N |
| $f_g$ | = | combination of terms, dimensionless |
| $H$ | = | microhardness, GPa |
| $h_b$ | = | bulk conductance, W/m$^2 \cdot$ K |
| $h_c$ | = | contact penetration depth, nm |
| $h_{\text{contact}}$ | = | contact conductance, W/m$^2 \cdot$ K |
| $h_j$ | = | joint conductance, W/m$^2 \cdot$ K |
| $I_g$ | = | gap conductance integral, dimensionless |
| $k$ | = | material conductivity, W/m$^2 \cdot$ K |
| $L$ | = | applied force, $\mu$N |
| $M$ | = | gas rarefaction parameter, m |
| $m$ | = | combined absolute asperity slope, rad |
| $n$ | = | plane index number |
| $P$ | = | apparent contact pressure, GPa |
| $\dot{Q}$ | = | joint heat transfer rate, W |
| $R_b$ | = | bulk resistance |
| $R_c$ | = | contact resistance, K/W |
| $R_g$ | = | gap resistance, K/W |
| $R_j$ | = | joint resistance, K/W |
| $S$ | = | contact stiffness, d$p$/d$h_c$ |
| $T$ | = | temperature, K |
| $t$ | = | final thickness, m |
| $t_0$ | = | original thickness, m |
| $Y$ | = | mean plane separation, m |
| $\alpha$ | = | tip constant, 1.168 for Berkovich tip |
| $\gamma$ | = | plasticity index |
| $\Delta T_j$ | = | joint temperature drop, K |
| $\Theta$ | = | see Eq. (24) |
| $\theta$ | = | scattering angle, deg |
| $\lambda$ | = | incident wavelength, m |
| $\nu$ | = | Poisson's ratio |
| $\sigma$ | = | effective surface roughness, $\sqrt{(\sigma_1^2 + \sigma_2^2)}$, m) |
| $\omega$ | = | uncertainty parameter |

*Subscripts*

| | | |
|---|---|---|
| $c$ | = | contact |
| $e$ | = | elastic |
| $g$ | = | gap |
| $i$ | = | index number, interface |
| $p$ | = | polymer |
| $r$ | = | reduced |
| $s$ | = | harmonic |
| 1, 2 | = | surface of solids 1 and 2 |

Presented as Paper 2005-760 at the AIAA Aerospace Sciences Meeting, Reno, NV, 10–13 January 2005; received 18 January 2005; revision received 13 July 2005; accepted for publication 13 July 2005. 

*Research Assistant, Mechanical Engineering Department.
†Associate Research Professor, Mechanical Engineering Department. Associate Fellow AIAA.
‡Regents Professor and Dietz Professor, Mechanical Engineering Department. Honorary Fellow AIAA.

## Introduction

WHEN thermal energy flows across an interface, there exists an opposition to its transfer due to microscale constrictions caused by contacting asperities. The contacting asperities can comprise metal/metal, metal/inorganic, or in this case metal/organic contacts; this same phenomenon will exist as long as a discontinuity at an interface is present. When the thermal energy flow is across two surfaces in contact, the opposition is called the thermal contact resistance. The thermal contact resistance is computed by knowing the heat rate across the two contacting surfaces and the temperature difference calculated from the respective surface temperatures,

$$R_j = (T_1 - T_2)/\dot{Q} \tag{1}$$

Thermal contact resistance plays a major role in almost all power-generating systems. Many design constraints are based on heat generation and the ability of the system to dissipate heat effectively. Computer chip packaging technology is a good example of the desire for maximum heat dissipation over a small area.

To allow a microprocessor to remain under its maximum operating temperature, heat sinks or heat pipes are employed to help in heat dissipation. The heat must flow from the chip through an adhesive or thermal interstitial material (TIM) to the heat sink or spreader. At every interface, the contact resistance to the heat flow

lowers the effective thermal conductance of the joints. As the thermal conductance is decreased, less heat is dissipated and the chip remains close to the maximum operating temperature. Factors such as efficiency, durability, and reliability can be affected by the heat dissipation.

Recently, polymers and organic materials have been employed to a greater extent in power-generating systems, and their greater use increases the interest in the thermophysical and mechanical properties of polymers. These properties may include thermal conductivity, heat capacity, Young's modulus, Poisson ratio, percent crystalline structure, microhardness if measurable, and the thermal contact resistance at the interface with other materials. Currently, two thermal contact models exist, that is, elastic and plastic, that encompass the entire thermal joint, that may be used to predict the thermal contact resistance. However, these models have been compared to a relatively selective group of polymers that are somewhat thick, for example, 2000 $\mu$m or greater. This study will eventually investigate the usability of these models ranging from 12 to 254 $\mu$m thickness. This analysis will be presented in a subsequent paper because the amount of experimental data is quite large.

## Literature Review

Miller and Fletcher[1] and Fletcher and Cerza[2] originally presented experimental studies for organic layers with an objective of evaluating the thermal conductance characteristics/performance of these types of material. The authors concluded that thermal conductance values of tested elastomers were lower than the thermal conductance of bare aluminum interfaces. However, they also observed that the addition of fillers, whether metallic or nonmetallic, produced higher thermal conductance value improvements than unfilled elastomers. In addition, experimentally gathered data for polyethylene materials over a range of pressures and interface temperatures resolved the effect of carbon filler loading and the effect of increasing temperature.

Ochterbeck et al.[3] investigated the effect on thermal joint conductance of various compounds applied directly onto a polyimide infrastructure. These compounds included several paraffin waxes, diamond-impregnated films, and metallic foils. In all instances, the experimental data showed an increase in thermal joint conductance over bare junctions; however, the greatest improvement or thermal performance increase was provided by the paraffin-based compound.

Marotta and Fletcher[4] investigated the thermal conductance of several commercially important polymers. Within the range of apparent interface pressure, the thermal conductance values indicated independence at moderate to high loading. For several thermoplastic polymers, which are soft and ductile, an increase in thermal joint conductance was measured at the higher apparent pressures, which was attributed to bulk material deflection. This was subsequently shown to be true by Bahrami et al.[5] when the experimental data were compared to a plastic deformation model for contacting asperities.

An experimental investigation by Mirmira et al.[6] revealed that the thermal joint conductance of several commercially available elastomeric materials became less dependent on apparent interface pressure. These values occurred as the interface loading increased significantly, with the bulk conductance becoming predominant at the high-pressure range (1–500 kPa). This work was later summarized by Marotta and Han.[7] In addition, for some filled silicone elastomeric materials, such as silver-coated copper powders and silver flakes, thermal conductance values indicated more independence from pressure due to increased rigidity from the powders and flakes incorporated within its structure. The authors also observed that the change in thermal conductance values was negligible with respect to increased mean interface temperature for several gasket materials.

Fuller and Marotta[8] developed an analytical model for the prediction of thermal joint conductance for both thermoplastic and elastomeric polymers placed between metallic solids. The assumptions included nominally flat contacting surfaces, uniform pressure distribution at the interface, elastic deformation of the polymer layer and asperities, and a vacuum environment. The analytical model employed the Greenwood and Williamson[9] definition for the elastic contact hardness to define a new polymer elastic hardness.

From the analytical model and polymer elastic hardness, Fuller and Marotta[8] were able to obtain a simple correlation for the dimensionless microscopic contact conductance:

$$h_c\sigma/k_s m = 1.49(2.3P/E_p m)^{0.935} \tag{2}$$

By defining the final thickness in terms of the strain, and the bulk thermal conductance with respect to the polymer thickness $t$ and thermal conductivity, the authors obtained a final expression for the joint conductance defined as

$$h_b = k_p/t \tag{3}$$

$$t = t_0(1 - P/E_p) \tag{4}$$

$$h_j = [1/h_{\text{contact},1} + t_0(1 - P/E_p)/k_p + 1/h_{\text{contact},2}]^{-1} \tag{5}$$

Experimental data from Marotta and Fletcher[4] and Fuller and Marotta[8] were compared to the joint conductance model, and very good agreement was achieved for the range of parameters employed in their studies.

Bahrami et al.[5] have also shown very good agreement between the experimental data gathered by the mentioned researchers and the plastic deformation assumption for contacting asperities. The joint resistance model was presented as

$$R_j = \frac{0.505H(\sigma/m)}{k_s F} + \frac{t_0(1 - P/E_p)}{A_a k_p} \tag{6}$$

where $F$ is the applied load and the remaining parameters are either mechanical or thermophysical properties. This model assumes that polymer microhardness can be measured for all polymers; however, this still must be demonstrated for polymer films or other polymer types as well, for example, elastomers.

If a fluid is present at the contacting interfaces, then the joint thermal resistance to heat flow that incorporates the bulk properties of the interstitial layer can be defined as

$$R_j = [1/R_{c,1} + 1/R_{g,1}]^{-1} + R_b + [1/R_{c,2} + 1/R_{g,2}]^{-1} \tag{7}$$

where $R_{c,1}, R_{c,2}, R_{g,1}$, and $R_{g,2}$ are the thermal contact resistances and the thermal gap resistances at each interface, respectively, and $R_b$ is again the thermal resistance due to the bulk properties of the layer. The thermal joint resistance is defined as the temperature drop across the entire joint divided by the total heat flow rate [Eq. (1)].

The thermal contact reistance and bulk resistance can be written as

$$R_{c,i} = 1/h_{\text{contact},i} A_a \qquad i \rightarrow 1\text{–}2 \tag{8}$$

$$R_b = 1/h_b A_a \tag{9}$$

$$R_{g,i} = 1/h_{g,i} A_a \qquad i \rightarrow 1\text{–}2 \tag{10}$$

Therefore, the thermal joint resistance can be rewritten in terms of thermal conductance as

$$h_j = 1/[1/(h_{\text{contact},1} + h_{g,1}) + 1/h_b + 1/(h_{\text{contact},2} + h_{g,2})] \tag{11}$$

Equation (11) is the generalized expression from which the overall joint conductance can be calculated; however, the complexity in computing the individual constituents makes this a very challenging task indeed.

Expressions (2) (elastic contacts, for polymers only) or the first term in expression (6) (plastic contacts) can be employed for the calculation of the contact conductance $h_c$ or its inverse, $R_c$, and bulk conductance $h_b$ from Eqs. (3) and (4). The gap conductance $h_g$ may be computed from gap conductance models first developed by Yovanovich et al.[10] The model assumes that the two surfaces in

contact are uniform in temperature and the interface gap consists of many elemental flux tubes of varying thermal resistances. The integration of these tubes over the nominally contacting area gives the overall gap conductance,

$$h_g = (k_g/\sigma) I_g \tag{12}$$

$$I_g = 1/(Y/\sigma + M/\sigma) \tag{13}$$

Expression (13) for $I_g$ is accurate to within 10% for large values of the dimensionless relative gap and gas parameter; however, its accuracy diminished considerably for small values. Therefore, Negus and Yovanovich[11] proposed a new correlation that incorporated a correction factor $f_g$ that modified the expression (13) for the integral function,

$$I_g = f_g/(Y/\sigma + M/\sigma) \tag{14}$$

A simple approximate expression for $f_g$ was derived as

$$f_g = 1.063 + 0.0471(4 - Y/\sigma)^{1.68}[In(\sigma/M)]^{0.84} \tag{15}$$

for $2 \leq Y/\sigma \leq 4$ and $0.01 \leq M/\sigma \leq 1$ and

$$f_g = 1.0 + 0.06(\sigma/M)^{0.8} \tag{16}$$

for $2 \leq Y/\sigma \leq 4$ and $1 \leq M/\sigma \leq \infty$.

For phase change materials or other types of filler materials present within the gap, instead of a gas, the overall gap conductance becomes

$$h_g = k_i/Y \tag{17}$$

The mean plane separation $Y$ or gap parameter is the distance between the mean planes passing through the two rough surfaces. This parameter is related to the effective rms surface roughness and asperity slope, contact pressure, and the interstitial material Young's modulus via the expression developed for elastomeric materials

$$Y/\sigma = \sqrt{2}\,\mathrm{erfc}^{-1}(2.3P/E_p m) \tag{18}$$

or for plastic deformation at the contacting asperties as

$$Y/\sigma = \sqrt{2}\,\mathrm{erfc}^{-1}(2P/H) \tag{19}$$

where $H_p$ is the microhardness of the softer contacting asperities.

Narh and Sridhar[12] gathered experimental thermal conductance data on polystyrene as a function of thickness at constant pressure and mean specimen temperatures (65 and 75°C). The authors noted that at temperatures slightly above the polymer's glass transition temperature, where the polymer's surface becomes relatively soft and ductile, the thermal contact resistance varied as a logarithmic function of pressure.

An in-depth review of enhancement TIM, grease-filled interstitial gaps for joints, and thermal conductance models was conducted by Savija et al.[13,14] In addition, Savija[15] conducted an investigation of thermal interface materials in the form of thin sheets of Grafoil GTA 005, 015, and 030. CHO-THERM 1671, just one of many polymeric materials with applications in microelectronic cooling, was also tested. In all tests, thermal resistance data were obtained for both loading and unloading cycles at interface pressures from 0.2 to 6.5 MPa. An interesting distinction between the two materials was the difference in applied pressure at which the onset of the bulk resistance would dominate over the interface contact resistance, 2 vs 4 MPa, respectively, for Grafoil GTA and CHO-THERM 1671.

A similar study was conducted by Marotta et al.[16] for the effect of interface pressure on thermal joint conductance for flexible graphite materials. An analytical model for the resistance across the joint incorporating a sheet of interstitial elastic material and gap filler such as a gas or phase change material was developed. The proposed joint model was compared to experimental data obtained for several commercially available graphite materials. The joint resistance ranged from 65.8 to 10.3 mm$^2$ K/W and showed good agreement with the proposed model.

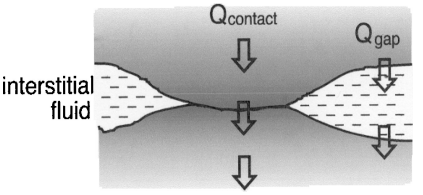


**Fig. 1 Microscopic view of contact interface in conforming rough surface.**

In general, experimental studies have been conducted for numerous interstitial materials with respect to their effect on thermal contact conductance. However, the applicability of analytical models to the prediction of joint conductance, and comparison to experimental data, is still in its infancy. At the present time, joint resistance models have only been investigated for a limited number of materials under vacuum conditions.

This study investigates the effect on thermal joint resistance for a metallic solid to interstitial layer joint caused by the variation of interface pressure for two different polymer films, that is, polyester and low-density polyethylene (LDPE) films, that are employed in several engineering applications. The test conditions included the use of air as the gap filler at the contacting surfaces. The presence of a gas at the interface provides a second avenue for heat flow through the interface, for example, vs a vacuum environment, as shown in Fig. 1.

## Experimental Program

The experimental facility and operations employed for the experimental portion of this study have been described in the published literature. Thus, a formal discussion will not be given here, but readers are encouraged to review the work of Marotta and Fletcher,[4] Fuller and Marotta,[8] and Savija[15] for greater details.

The joint models highlighted in the preceding section will be compared to the experimental data for these polymeric films (LDPE and polyester) in a subsequent paper because the main emphasis of this paper is solely experimental.

### Thermal Joint Conductance

The joint conductance data are shown plotted as a function of the joint apparent pressure in Figs. 2–7. Figures 2–7 show the effects of applied pressure and mean polymer film temperature on thermal joint conductance values. The contacting interface that comprises part of the thermal joint consists of the polymeric film and National Institute of Standards and Technology (NIST) 8421 electrolytic iron as the metallic surface in intimate contact. Each polymeric specimen can be characterized by a level of crystallinity and by what portion of the crystalline structure comprises low-density mers or low degree of polymerization. This particular attribute will influence the observed joint conductance characteristics while being subjected to the range of pressures and interface temperatures already stated. The crystallinity analysis via high-angle x-ray diffraction will be shown in a subsequent section and could shed light/insight into the nature of the deformation behavior of the film.

Figures 2–4 present the thermal joint conductance as a function of apparent pressure for LDPE samples 1–3 during a loading cycle; each was subjected to three different interface temperatures. Very little deviation in joint conductance at very high interface pressures is cleary shown with differences observed for the lighter pressures. However, a shift in behavior can be seen all LDPE specimens, especially as the mean interface temperature is elevated higher than the glass temperature, $T_g$ (~65°C). A reversal in joint conductance for all specimens with respect to temperature was observed as $T_g$ was approached. Glass transition temperature is that temperature at which the polymer's thermal expansion coefficient is comparable to that of a liquid. Below $T_g$, the polymer material is a rigid solid, and above $T_g$ it is a supercooled liquid. Significant changes in mechanical and

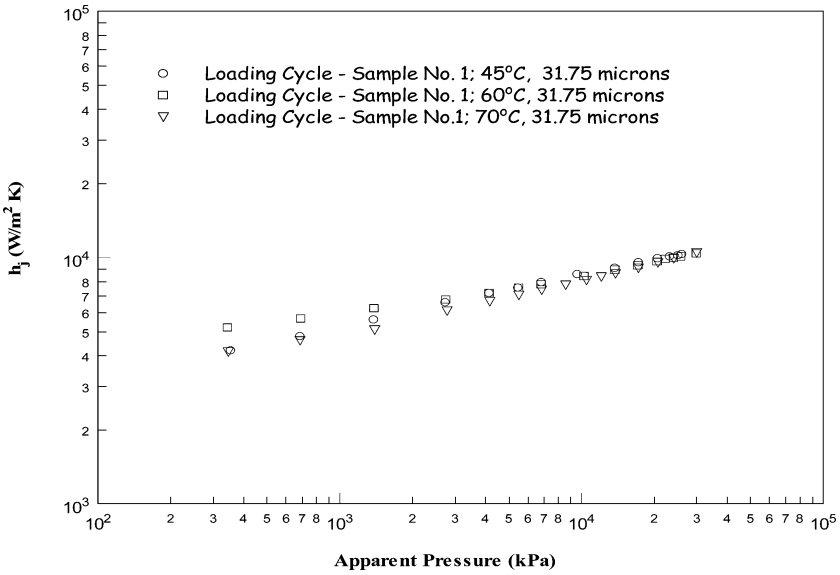


**Fig. 2 Thermal Conductance as function of applied pressure for LDPE specimen 1.**

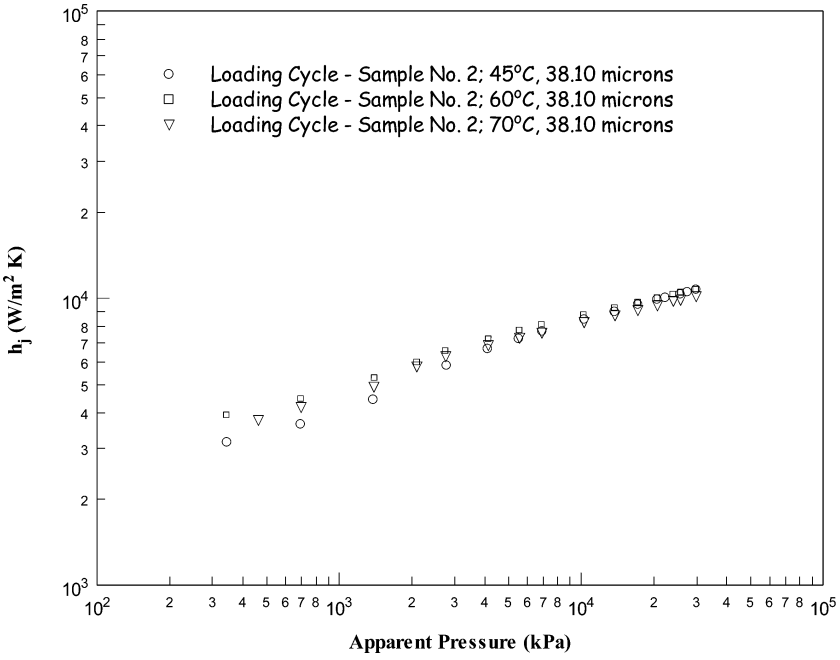


**Fig. 3 Thermal conductance as function of applied pressure for LDPE specimen 2.**

thermophysical properties, such the Youngs modulus and thermal conductivity, occur near and above this temperature.

The reason for this shift in behavior might also lie in the deformation mechanism that may be occurring. Therefore, to answer whether a change in mode is occurring or not, experimental data for thermal joint conductance for loading and unloading (one complete cycle) may provide some clues.

Figure 5 shows the cycle for two of the three LDPE specimens for the interface temperature of 45°C. The loading and unloading data indicate that specimen 1 is acting elastically with respect to bulk-layer deformation mode. Whether the contacting asperities are deforming elastically can not be determined from these data, but nanoindention experiments will shed light with respect to this question (next section). Clearly, the experimental data indicate a plastic deformation for specimen 2 with a tremendous shift in conductance as the load is removed, although this was not the case for specimen 1. Again, the polymeric structure or level of crystallinity might lend insight, and this can be accomplished by high-angle x-ray diffractions plots. These plots will enable the determination of not only the percentage crystallinity of the film, but in addition, the atomic spacing or distance between adjoining chains within the crystalline cluster.

Mylar®, which is an extraordinarily strong polyester film that grew out of the development of Dacron, is a thermoplastic made from ethylene glycol and dimethyl terephtha that ultimately produces polyethylene terephthalate. This film is employed for its high tensile strength, transparency, and electrical insulation that make it ideal in high voltage film capacitors. Moreover, Mylar thermophysical and mechanical properties make it suitable for applications in electronic, magnetic media, imaging/graphics, and other packaging markets. Therefore, characterizing thermal joint conductance performance is an important factor, which will enable better packaging schemes.

Figures 6 and 7 show the thermal joint conductance as a function of applied interface pressure for a 12-$\mu$m film of Mylar. These experimental runs were conducted at temperatures below and well above its glass transition ($T_g = 70^\circ$C) temperature, respectively. In each

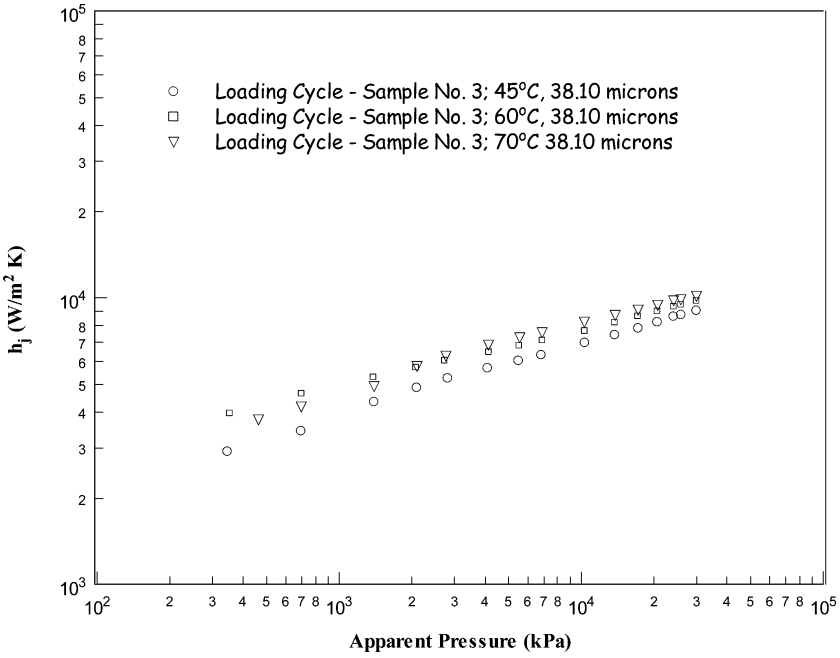


**Fig. 4 Thermal conductance as function of applied pressure for LDPE specimen 3.**

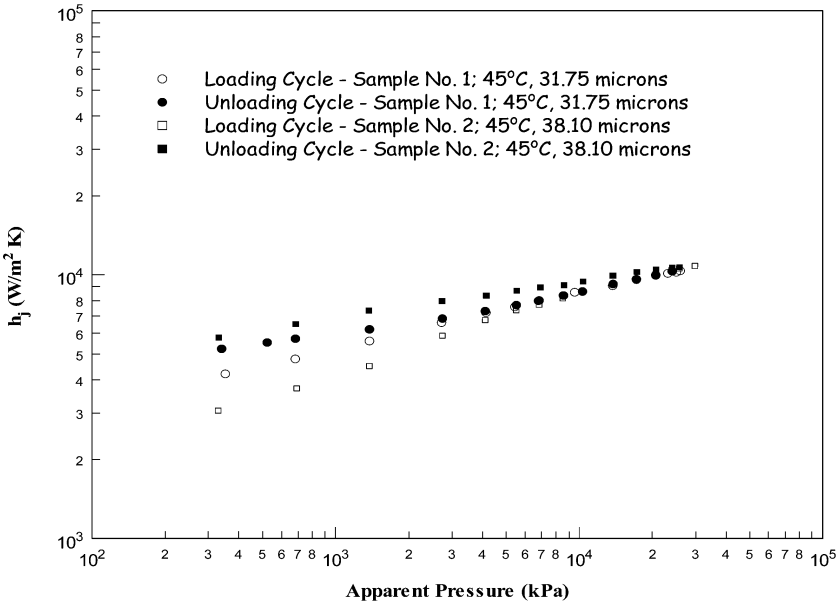


**Fig. 5 Thermal conductance cycle as function of applied pressure for LDPE specimens 1 and 2.**

case, the experiments were conducted with a full cycle of loading and unloading of the film. Note that the film does behave elastically at room temperature, whereas slight plastic deformation can be observed at the mean interface temperature of 100°C. It is known that the polymer film's elastic modulus decreases rapidly as the $T_g$ temperature, ~70°C, is approached; thus, the film becomes more fluidlike rather than a semirigid solid.

This fluidlike behavior at elevated temperatures can be attributed to the weak, secondary bonds, for example, van der Waals, or dipole attraction. In fact, Fig. 7 seems to show the typical characteristics of nonlinear elasticity with a high strain modulus at high loads, due to covalent bonding, and low strain modulus at low loads, due to secondary bonding effects. This behavior is similar to elastomeric polymers where the uncoiled polymer molecules recoil to their original length on removal of the applied stress.

The degree of bulk plastic deformation for the polyester film can be partially attributed to its directional stretching process and subsequent biaxial oriented structure. This stretching process rearranges the polyester (PET) molecules into an ordered structure that substantially improves the film's mechanical properties and thermophysical properties as well.

### High-Angle X-Ray Diffraction

The technique most commonly used to determine the structure of a new material is x-ray diffraction. Diffraction is the result of radiation being scattered by a regular array of scattering centers. As a result, x-ray diffraction is capable of characterizing crystalline structure in inorganic solids, as well as organic materials such as polymers. For diffraction to occur, x-ray beams scattered off adjacent crystal planes must be in phase. If not, destructive interference of waves occurs and essentially no scattering intensity is observed. At the precise geometry for constructive interference, the difference in path length between adjacent x-ray beams can be described by the Bragg equation,

$$n\lambda = 2d \sin\theta \tag{20}$$

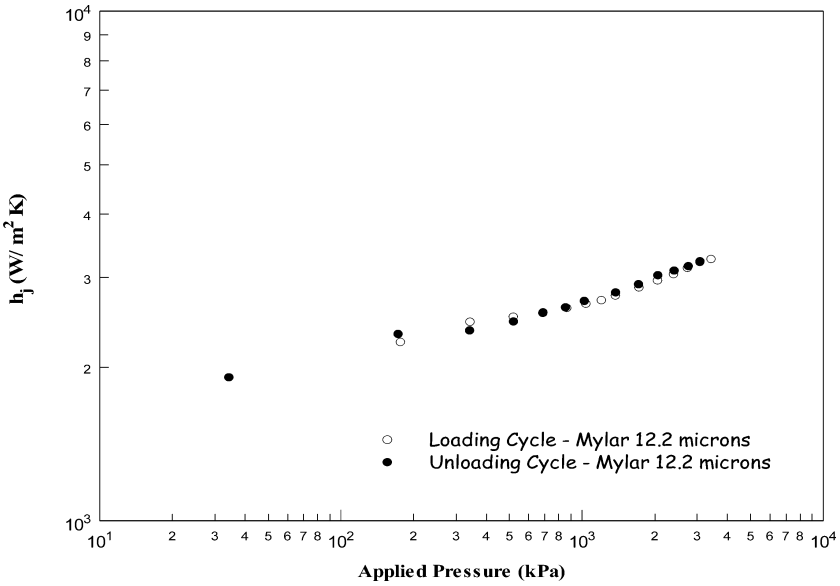


**Fig. 6 Thermal joint resistance as function of applied pressure for polyester specimen (Mylar) for mean interface temperature at 50°C.**

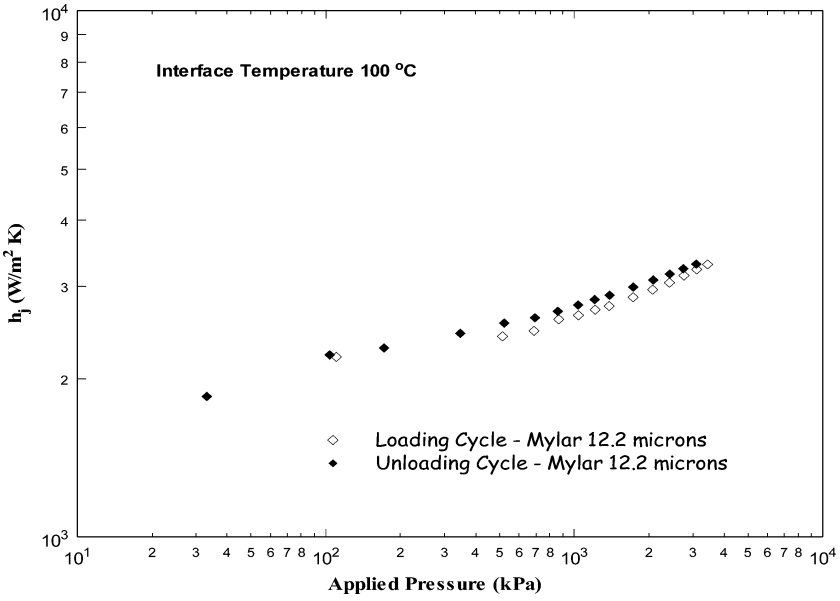


**Fig. 7 Thermal joint resistance as function of applied pressure for polyester specimen (Mylar) for mean interface temperature at 100°C.**

The angle $\theta$ of scattering is referred to as the Bragg angle and the angle $2\theta$ is referred to as the diffraction angle because that is the angle measured experimentally. Therefore, with the use of a high-angle x-ray diffractometer, an electromechanical scanning system, the diffracted radiation intensity of the polymeric films can be monitored electronically by a mechanically driven radiation detector. These experimental results are shown in Figs. 8–11. The percent crystallinity can be computed from the areas underneath the peak intensities to the overall area underneath the scan. High angle x-ray diffraction measurements for these polymer films indicate a higher percent crystallinity for LDPE 3, that is, 59%, vs the other two polymeric films, LDPE 1 and No. 2, 43 and 51%,respectively.

The computed crystallinity for PET film was experimentally determined to be much higher than the three LDPE films; this value was computed to be approximately ~83%. Although it seems that greater plastic deformation can be observed for LDPE with increased percent crystallinity, PET seems to indicate a lesser degree of influence on deformation mode caused by its crystalline structure.

Whereas these higher degrees of crystallinity may help explain the observed decrease in joint conductance for LDPE, what exact mechanisms are involved and how they influence overall joint conductance is still unclear, but is a seed for future research into polymer conductance.

The role of amorphorous vs crystalline areas within the polymer's overall structure needs to be investigated as well if one hopes to understand the effects on joint conductance and, ultimately, contact conductance at the interface between the polymeric material and solid metal.

### Nanoindenter Studies

Although the use of thermal joint conductance data might provide insight into the bulk deformation mode of the polymeric films, microscopic deformation at the contacting asperities can not be deduced.

The use of a nanoindenter will not only provide the characteristic microhardness of the film both at the surface and interior bulk, but, in addition, provide the elastic Young's modulus and a level of deformation, which can be described as either purely elastic, purely plastic, or elastoplastic.

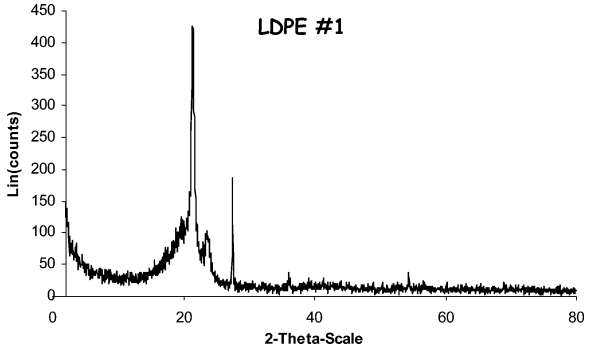


**Fig. 8 X-ray diffraction of LDPE 1.**

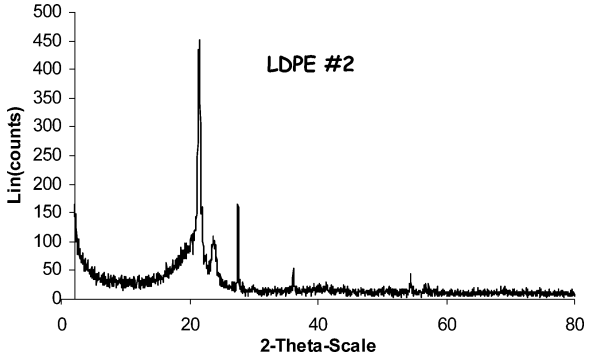


**Fig. 9 X-ray diffraction of LDPE 2.**

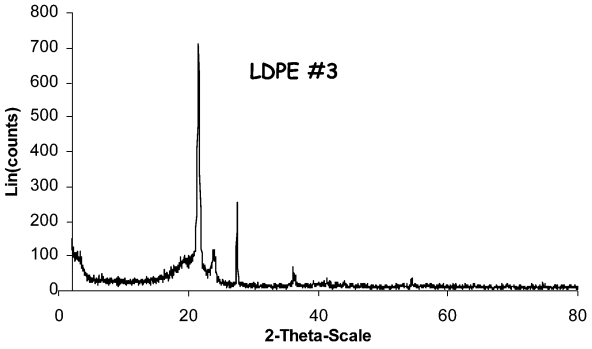


**Fig. 10 X-ray diffraction of LDPE 3.**

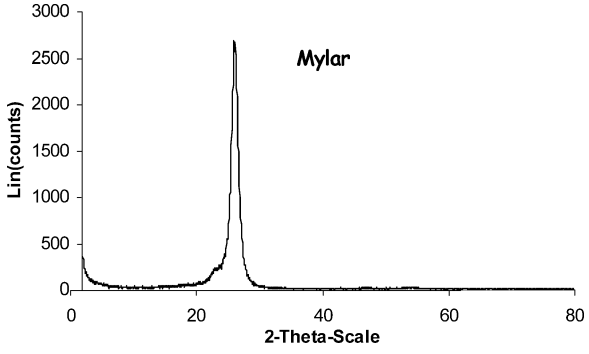


**Fig. 11 X-ray diffraction of PET (Mylar).**

Figures 12a and 12b show the experimental data for the reduced Young's modulus $E_r$ and microhardness as a function of indenter depth for LDPE specimen 1. Figures 13a and 13b show the experimental data for the reduced Young's modulus $E_r$ and microhardness as a function of indenter depth for LDPE specimen 2, whereas Figs. 14a and 14b show the same experimental data for LDPE specimen 3.

Figures 15a and 15b show the experimental data for the reduced Young's modulus $E_r$ and microhardness as a function of indenter

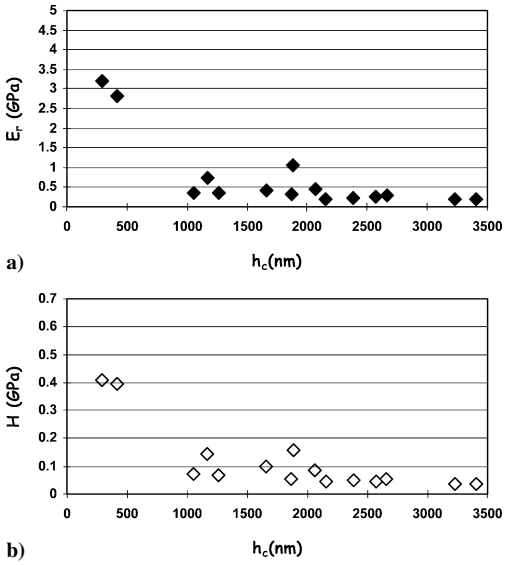


**Fig. 12 LDPE 1: a) Young's modulus and b) microhardness as a function of indenter depth.**

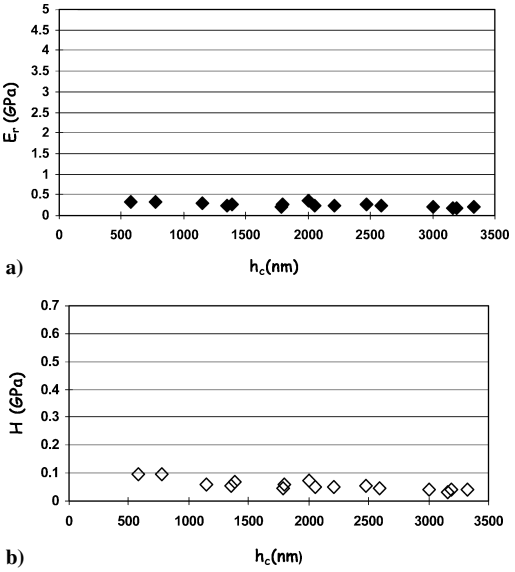


**Fig. 13 LDPE 2: a) Young's modulus and b) microhardness as a function of indenter depth.**

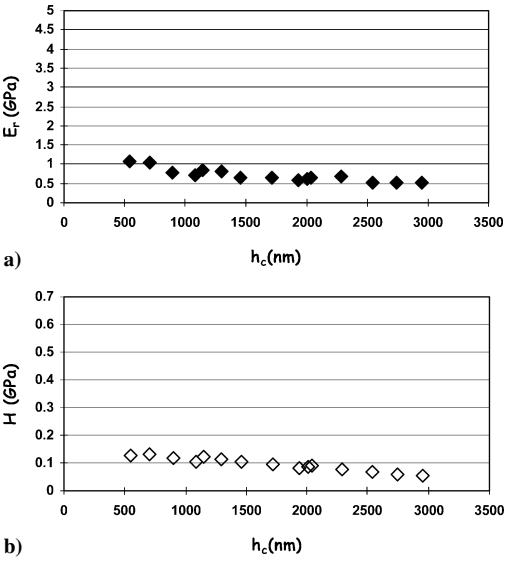


**Fig. 14 LDPE 3: a) Young's modulus and b) microhardness as a function of indenter depth.**

**Table 1 Mechanical data**

| Film | $E_r$ (1 $\mu$m), GPa | $H$ (1 $\mu$m), GPa | $E_r$ (3 $\mu$m), GPa | $H$ (3 $\mu$m), GPa | $\gamma$ | $H_c$ |
|---|---|---|---|---|---|---|
| 1 | 0.50 | 0.095 | 0.25 | 0.04 | 0.88 | 0.047 |
| 2 | 0.30 | 0.06 | 0.20 | 0.04 | 1.09 | 0.024 |
| 3 | 0.80 | 0.12 | 0.50 | 0.06 | 0.67 | 0.078 |
| Mylar | 4.00 | 0.50 | —— | —— | 1.42 | 0.153 |

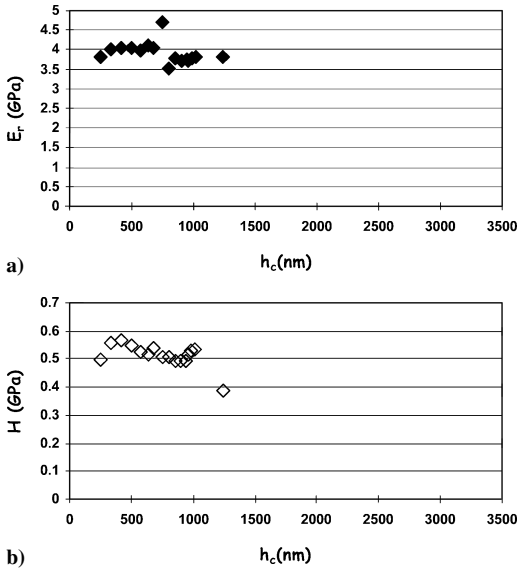


**Fig. 15 Mylar film 12.2 $\mu$m thick: a) Young's modulus and b) microhardness.**

depth for the Mylar film. It is quite interesting that the size effect observed for the low-density polyethylene polymer films is absent for the Mylar film. The computed crystallinity, as shown by Fig. 11, for PET film is much higher than the three LDPE films; therefore, this higher value could possibly explain this observation, but one can not definitely be sure without further experimentation. However, if the values at shallow indentations are ignored because of size effects, then a trend can be observed between $E_r$ and $H$ with respect to film percent crystallinity.

In each case, the experimental data indicate an indenter size effect with respect to the projected/true contact area at maximum load/penetration of the Berkovich indenter, which is a three-sided pyramidal tip. The following equation is typically used to obtain the elastic modulus $E_r$ from the unloading portion of the curve:

$$E_r \Big/ (1 - \nu^2) = S \Big/ \alpha \sqrt{A_t} \tag{21}$$

where $S = \mathrm{d}P/\mathrm{d}h_c$ and is the contact stiffness obtained from the initial portion of the unloading curve. It is well-documented that there exists an indentation size effect in the low to submicrometer range; this has been shown in polymers, metals, diamondlike carbon, and ceramics[17–22]. Indentation-size effect is the reduction in material hardness with increasing indentation depth in the low to submicrometer range. This effect has been explained on the basis of geometrically necessary dislocations within crystalline materials, but has been applied to amorphous materials as well. The indentation size effect has been shown to correlate well with surface roughness.

The experimental data for nanoindentations were gathered with a Hysitron TriboIndenter®, which employs a three-plate capacitive transducer that acts as both as an actuator and sensor by applying and measuring normal and lateral loads while indenting. The force is applied electrostatically while the displacement is simultaneously monitored as a change in capacitance.

Tables 1 and 2 highlight the relationship between the mechanical properties measured at 1- and 3-$\mu$m indentation depth so that the size effect phenomenon is removed. It seems from this limited data set

**Table 2 Metrology and Thermophysics Data**

| Film | $R_q$, $\mu$m | $m_q$, rad | $k$, W/m·K | $T_g$, °C | $t_0$, $\mu$m | Crystal, % |
|---|---|---|---|---|---|---|
| 1 | 3.68 | 0.215 | 0.29 | 60–65 | 31.7 | 43 |
| 2 | 1.84 | 0.183 | 0.35 | 60–65 | 38.1 | 51 |
| 3 | 4.79 | 0.225 | 0.31 | 60–65 | 38.1 | 59 |
| Mylar | 0.19 | 0.088 | 0.155 | 70 | 12.2 | 83 |

that properties tend to increase with increasing crystallinity except for LDPE 2, where no difference is observable from LDPE 1. At the present time, an explanation for this discontinuity for LDPE 2 is unknown. For future modeling purposes, metrology data for each polymeric film are included as well. (These parameters will be utilized in a subsequent paper for modeling purposes.)

A priori prediction of the deformation can be obtained with the use of a parameter first developed by Mikic.[23] He proposed a plasticity index to determine the mode of deformation,

$$\gamma = H/E'm \tag{22}$$

On the basis of Mikic's analysis, he developed a criterion for surfaces in contact. If the value of $\gamma \geq 3.0$, then the deformation mode is 90% elastic for contact asperities, and for values of $\gamma \leq 0.33$, the deformation mode is such that 90% of contacting asperities will deform plastically. In fact, if the value of the plasticity index is between these two values, then the possibility exists that both modes of deformation could occur to varying degrees of probability: $0.33 \leq \gamma \leq 3.0$.

Therefore, with this criterion in mind, the mode of deformation for these types of polymer film is not purely plastic or elastic, with the possibility of elastoplastic deformation governing among the contacting asperities.

Fuller and Marotta[8] developed an elastic model for calculating the thermal contact conductance of polymer/metal interfaces and found very good agreement between experimental data and their model,

$$H_e = E_p m/2.3 \tag{23}$$

However, it has been noted by Bahrami et al.[5] that possibilities exist or can arise where the elastic hardness parameter $H_e$ is greater than the plastic microhardness $H_{\mathrm{mic}}$. As shown within Table 1, the elastic hardness values are all below the polymer film's microhardness, $H_{\mathrm{mic}}$, therefore, not violating this possibility. This can occur if one does not employ the correct mechanical and metrology data in determining the parameter (which includes the plasticity index as well) without direct measurements such as a nanoindenter. Nanoindenter measurements allow the correct measurement of surface microhardness and polymer Young's modulus very precisely, therefore, minimizing the possibility of this occurring.

A mode for microdeformation at the asperity level can be gleaned from the family of curves shown in Fig. 16 for Mylar. Similar curves can be seen by the LDPE films as well; however, only this polymer type was chosen to be shown. It becomes apparent from these curves that the deformation mode is elastoplastic because the original values on its return are not along the initial loading curve. One can quantify the degree of elastic to plastic deformation from penetration depths shown for each maximum load curve. Each curve seems to indicate a two-thirds to one-third split in plastic to elastic deformation, respectively, for this particular film. These ratios can be computed from the indenter penetration depths up to the maximum

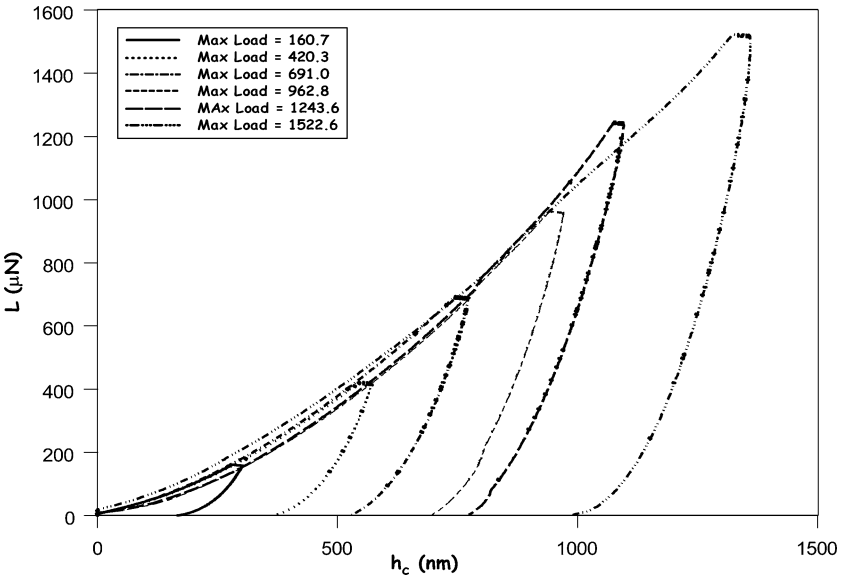


**Fig. 16 Load vs indenter penetration depth for PET film (Mylar).**

loading. A fully rigid plastic material would cause the unloading curve to drop vertical downward to zero load at the maximum indenter depth. An elastic material would cause the unloading curve to return to zero load along the same loading curve. An elastic–plastic material causes the unloading curve to reach zero somewhere in between these two extreme values.

Therefore, the ratio of maximum indenter depth possible to the actual indenter depth of the unloading curve at zero loading can provide the amount of plastic deformation. Interestingly, these values seem not to be influenced by the level of maximum loading applied, remaining fairly constant throughout the spectrum of maximum loads. This information indicates that an appropriate elastoplastic deformation model for asperity contact would be more appealing than just a singular mode for thermal contact modeling. (This will also be explored in a subsequent paper.)

To validate the measured mechanical and thermal properties, the experimental thermal conductance data can be plotted as dimensionless thermal resistance as a function of applied interface pressure. The thermal circuit for the polymeric material placed in between contacting surfaces can be described as

$$R_j = R_b + 2R_i \tag{24}$$

If the expression is divided by the bulk resistance of the polymeric film and rearranged, then the following expression results:

$$\Theta = R_j/R_b = 1 + 2 \cdot (R_i/R_b) \tag{25}$$

If the data are plotted against applied interface pressure, then at very high pressures the interface resistance $R_i$ becomes negligible compared to $R_b$. Therefore, the second term on the right-hand side of expression (24) tends toward zero, and the following simple expression results:

$$R_j/R_b = 1 \tag{26}$$

with the bulk thermal resistance calculated from the inverse of expression (9) multiplied by the apparent area. Equation (4) is used to quantify the variation of thickness in response to apparent contact pressure. Figures 17–19 show the results of the application of Eq. (24) to these polymeric films. Figures 17–19 each show the dimensionless parameter $\Theta$ tends toward 1 at high applied interface pressure, indicating negligible thermal interface resistance at the metal/polymer interface and bulk resistance dominating at these conditions.

Thermal, mechanical, and morphology studies have been conducted in an attempt to shed greater insight on the thermal and mechanical behavior of two widely used polymeric films. To enable thermal conductance modeling efforts to span into nontraditional

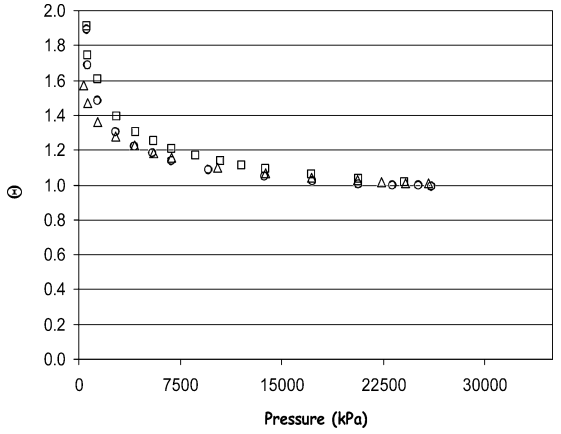


**Fig. 17 Dimensionless thermal resistance as function of applied interface pressure for specimen LDPE 1: ○, 45°C; △, 60°C; and □, 70°C.**

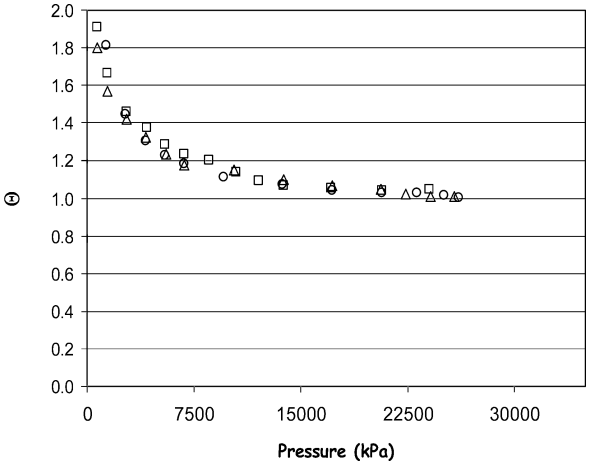


**Fig. 18 Dimensionless thermal resistance as function of applied interface pressure for specimen LDPE 2: ○, 45°C; △, 60°C; and □, 70°C.**

materials beyond metals and into interstitial materials, whether for enhancement or not, then experimental studies of these materials need to be conducted; this was the key goal of this investigation.

### Uncertainty Analysis

The uncertainties in the various quantities that are used in calculating thermal contact conductance can be combined to determine the overall relative uncertainty in the reported thermal conductivity

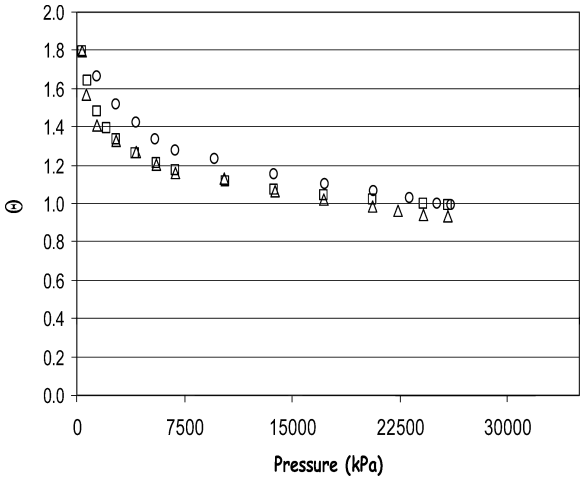


**Fig. 19 Dimensionless thermal resistance as function of applied interface pressure for specimen LDPE 3: ○, 45°C; △, 60°C; and □, 70°C.**

and thermal contact conductance data. The techniques described by Kline and McCintock[24] have been employed to calculate the overall relative uncertainty for thermal conductivity and thermal contact conductance. Equation (26) provides the means to determine the uncertainty in the thermal conductance, which involves the uncertainty in heat rate, cross-sectional area, and temperature drop across the interface as

$$\omega_h/h = \sqrt{(\omega_{\dot{Q}}/\dot{Q})^2 + (\omega_A/A_c)^2 + \left[\omega_{T_1}\big/(T_1 - T_2)\right]^2 + \left[\omega_{T_2}\big/(T_1 - T_2)\right]^2} \tag{27}$$

The uncertainty in heat rate $\dot{Q}$ and $A$ can be computed similarly. The average overall uncertainty in the thermal joint conductance was the accumulation of the uncertainties of the individual parameters from which the joint conductance was computed. These uncertainties included the T-type thermocouples (special limit of error) for $T_1$ and $T_2$ as $\pm 0.5$°C, the uncertainty in the cross-sectional area $A$ of $\pm 20.1 \times 10^{-6}$ m$^2$, the uncertainty in the heat rate $\dot{Q}$ of $\pm 1.0$ W, the NIST iron thermal conductivity $k_{\text{iron}}$ uncertainty of $\pm 1.10$ W/m · K, and the spacing between thermal couple readings, $\pm 5.1 \times 10^{-5}$. Therefore, the computed values for LDPE 2 at the interface temperature of 70°C ranged from 5.5 to 10.3% that is, 345.0–30,000 kPa (50–4350 psi), respectively. At an interface temperature of 45°C, the computed values for LDPE 2 ranged from 9.9 to 17.3%, respectively, for the same pressure range. The higher computed uncertainty at the lower interface temperature was due to the lower temperature drop at the joint. Similar values for uncertainty were obtained for LDPEs 1 and 3.

## Summary

One objective of the present investigation was to investigate experimentally LDPE and Mylar film types for thermal joint conductance with thickness values that ranged from 38.1 to 12.2 $\mu$m; these thicknesses were lower than what has been previously measured. Interface pressures were varied from a low of 103.4 kPa (15 psi) to a very high of 23,774.5 kPa (3450 psi), which are similar to interface pressures typical of injection molding machines.

In each of the experimental tests, the ambient fluid was air at atmospheric conditions. Thermal joint conductance data were obtained for a polymer film/metal joint.

Nanoindentation measurements indicate an elastoplastic mode for the asperity contact deformation, whereas elastic deformation prevails for the bulk films when the temperature is below the polymer's glass transition temperature $T_g$; plastic deformation seems to become prevalent above $T_g$. Surface metrology and film morphology data are also included to correlate film morphology (percent crystallinity) with film and asperity deformation and to incorporate metrology results into future modeling endeavors.

## References

[1]Miller, R. G., and Fletcher, L. S., "Thermal Conductance of Gasket Materials for Spacecraft Joints," AIAA Paper 73-119, Jan. 1973.

[2]Fletcher, L. S., and Cerza, M. R., "Thermal Conductance and Thermal Conductivity of Selected Polyethylene Materials," AIAA Paper 75-187, Jan. 1975.

[3]Ochterbeck, J. M., Fletcher, L. S., and Peterson, G. P., "Evaluation of Thermal Enhancement Films for Electronic Packages," *Proceedings of the 9th International Heat Transfer Conference*, Vol. 5, Aug. 1990, pp. 445–451.

[4]Marotta, E. E., and Fletcher, L. S., "Thermal Contact Conductance of Selected Polymeric Materials," *Journal of Thermophysics and Heat Transfer*, Vol. 10, No. 2, 1996, pp. 334–342.

[5]Bahrami, M., Yovanovich, M. M., and Marotta, E. E., "Modeling of Thermal Joint Resistance of Polymer-Metal Rough Interfaces," IMECE2004-60131, Proceeding of American Society of Mechanical Engineers International Mechanical Engineers Conference, Nov. 2004.

[6]Mirmira, S. R., Marotta, E. E., and Fletcher, L. S., "Thermal Contact Conductance of Elastomeric Gaskets," *Journal of Thermophysics and Heat Transfer*, Vol. 12, No. 3, 1997, pp. 454–456.

[7]Marotta, E. E., and Han, B., "Thermal Control of Interfaces for Microelectronic Packaging," *Material Society Symposium Proceedings*, Vol. 515, Materials Research Society, Warrendale, PA, 1998, pp. 215–225.

[8]Fuller, J. J., and Marotta, E. E., "Thermal Contact Conductance of Metal/Polymer Joints: An Analytical and Experimental Investigation," *Journal of Thermophysics and Heat Transfer*, Vol. 15, No. 2, 2001, pp. 228–238.

[9]Greenwood, J. A., and Williamson, J. B., "Contact of Nominally Flat Surfaces," *Proceedings of the Royal Society of London*, Vol. A295, 1966, pp. 300–319.

[10]Yovanovich, M. M., DeVaal, J. W., and Hegazy, A. A., "A Statistical Model to Predict Thermal Gap Conductance Between Conforming Rough Surfaces," AIAA Paper 82-0888, June 1982.

[11]Negus, K. J., and Yovanovich, M. M., "Correlation of the Gap Conductance Integral for Conforming Rough Surfaces," *Journal of Thermophysics and Heat Transfer*, Vol. 2, No. 3, 1988, pp. 279, 280.

[12]Narh, K. A., and Sridhar, L., "Measurement and Modeling of Thermal Contact Resistance at a Plastic Metal Interface," *55th Annual Technical Conference*, ANTEC 97, Society of Plastics Engineers, Brookfield, CT, 1997, pp. 2273–2277.

[13]Savija, I., Culham, R., Yovanovich, M. M., and Marotta, E. E., "Review of Thermal Conductance Modeling Procedures for Interfaces Incorporating Enhancement Materials," *Journal of Thermophysics and Heat Transfer*, Vol. 17, No. 1, 2003, pp. 43–52.

[14]Savija, I., Culham, R., Yovanovich, M. M., and Marotta, E. E., "Thermal Joint Resistance Model for Conforming Rough Surfaces with Grease Filled Interstitial Gaps," *Journal of Thermophysics and Heat Transfer*, Vol. 17, No. 2, 2003, pp. 278–281.

[15]Savija, I., "Methods for Determining Thermophysical Properties of Thermal Interface Materials," M.A.S. Thesis, Mechanical Engineering, Univ. of Waterloo, Waterloo, Canada, June 2002.

[16]Marotta, E., LaFontant, S., McClafferty, D., Mazzuca, S., and Norley, J., "The Effect of Interface Pressure on Thermal Joint Conductance for Flexible Graphite Materials: Analytical and Experimental Study," *Proceedings of the 8th Intersociety Conference on Thermal and Thermophysical Phenomena in Electronic Systems*, 2002, pp. 663–670.

[17]Pethica, J. B., Hutchings, R., and Oliver, W. C., "Hardness Measurements at Penetration Depths as Small as 20-nm," *Philosophical Magazine A–Physics of Condensed Matter Structured Defects and Mechanical Properties*, Vol. 48, No. 4, 1983, p. 593.

[18]Mott, B. W., *Micro-indentation hard testing*, Butterworths, London, 1956.

[19]Gane, N., and Cox, J. M., "Micro-Hardness of Metals at very Low Loads," *Philosophical Magazine Letters*, Vol. 22, 1970, p. 881.

[20]Sangwal, K. J., "Microhardness of As-Grown and Annealed Lead Sulfide Crystals," *Journal of Material Science*, Vol. 24, 1989, p. 1128.

[21]Cheng, Y. T., and Cheng, C. M., "Scaling, Relationships for Indentation Measurements," *Philosophical Magazine A–Physics of Condensed Matter Structured Defects and Mechanical Properties*, Vol. 82, No. 10, 2002, pp. 1821–1829.

[22]Krell, A., and Schadlich, S., "Nano-Indentation Hardness of Sub-Micrometer Alumina Ceramics," *Material Science and Engineering A–Structural Materials Properties Microstructure and Processing*, Vol. 307, No. 1–2, 2001, pp. 172–181.

[23]Mikic, B. B., "Thermal Contact Conductance; Theoretical Considerations," *International Journal of Heat and Mass Transfer*, Vol. 17, 1974, pp. 205–214.

[24]Kline, S. J., and McClintock, E A., "Describing Uncertainties in Single-Sample Experiments," *Mechanical Engineering*, Vol. 75, No. 1, 1953, pp. 3–8.